Integrative and Comparative Biology, volume 51, number 1, pp. 158–175
doi:10.1093/icb/icr020

SYMPOSIUM

Testing Biomimetic Structures in Bioinspired Robots: How Vertebrae Control the Stiffness of the Body and the Behavior of Fish-Like Swimmers

John H. Long Jr,[1,*,†,‡,§] Nicole M. Krenitsky,[§,¶] Sonia F. Roberts,[†,§] Jonathan Hirokawa,[†,§] Josh de Leeuw[§] and Marianne E. Porter[*,§]

*Department of Biology, Vassar College, Poughkeepsie, New York, USA; [†]Cognitive Science Program, Vassar College, Poughkeepsie, New York, USA; [‡]Neuroscience and Behavior Program, Vassar College, Poughkeepsie, New York, USA; [§]Interdisciplinary Robotics Research Laboratory, Vassar College, Poughkeepsie, New York, USA; [¶]Science, Technology, and Society Program, Vassar College, Poughkeepsie, New York, USA

From the symposium "Bioinspiration: Applying Mechanical Design to Experimental Biology" presented at the annual meeting of the Society for Integrative and Comparative Biology, January 3–7, 2011, at Salt Lake City, Utah.

[1]E-mail: jolong@vassar.edu

Synopsis Our goal is to describe a specific case of a general process gaining traction amongst biologists: testing biological hypotheses with biomimetic structures that operate in bioinspired robots. As an example, we present MARMT (mobile autonomous robot for mechanical testing), a surface-swimmer that undulates a submerged biomimetic tail to power cruising and accelerations. Our goal was to test the hypothesis that stiffness of the body controls swimming behavior and that both stiffness and behavior can be altered by changes in the morphology of the vertebral column. To test this hypothesis, we built biomimetic vertebral columns (BVC) outfitted with variable numbers of rigid ring centra; as the number of centra increased the axial length of the intervertebral joints decreased. Each kind of BVC was tested in dynamic bending to measure the structure's apparent stiffness as the storage and loss moduli. In addition, each kind of BVC was used as the axial skeleton in a tail that propelled MARMT. We varied MARMT's tail-beat frequency, lateral amplitude of the tail, and swimming behavior. MARMT's locomotor performance was measured using an on-board accelerometer and external video. As the number of vertebrae in the BVC of fixed length increased, so, too, did the BVC's storage modulus, the BVC's loss modulus, MARMT's mean speed during cruising, and MARMT's peak acceleration during a startle response. These results support the hypothesis that stiffness of the body controls swimming behavior and that both stiffness and behavior can be altered by changes in the morphology of the vertebral column.

Introduction

The mechanical design of a biological system is best understood in the context of the functioning organism. Live organisms, however, come with practical constraints: complexity, variability, and impermanence. To overcome these constraints, many researchers employ a new kind of physical model for biomechanical testing: robots that use biomimetic structures to enable behavior. As the shape, size, or mechanical properties of the structure are varied, the response of the robot is measured as a change in locomotor performance or behavior. Working with robots, researchers gain control over motor outputs and physical properties. This experimental control allows for stronger inference of the causal mechanisms connecting structure, mechanical properties, and locomotor performance (Fig. 1).

This approach is an extension and integration of the methodologies of biorobotics (Webb 2001, 2006; Webb and Consi 2001) and physical modeling in biomechanics with self-propelled robotic models (McHenry et al. 1995; Brooks 2001; Lauder and Madden 2006; Lauder et al. 2007; Tangorra et al. 2007). The specific hypothesis that we test

Advanced Access publication May 15, 2011

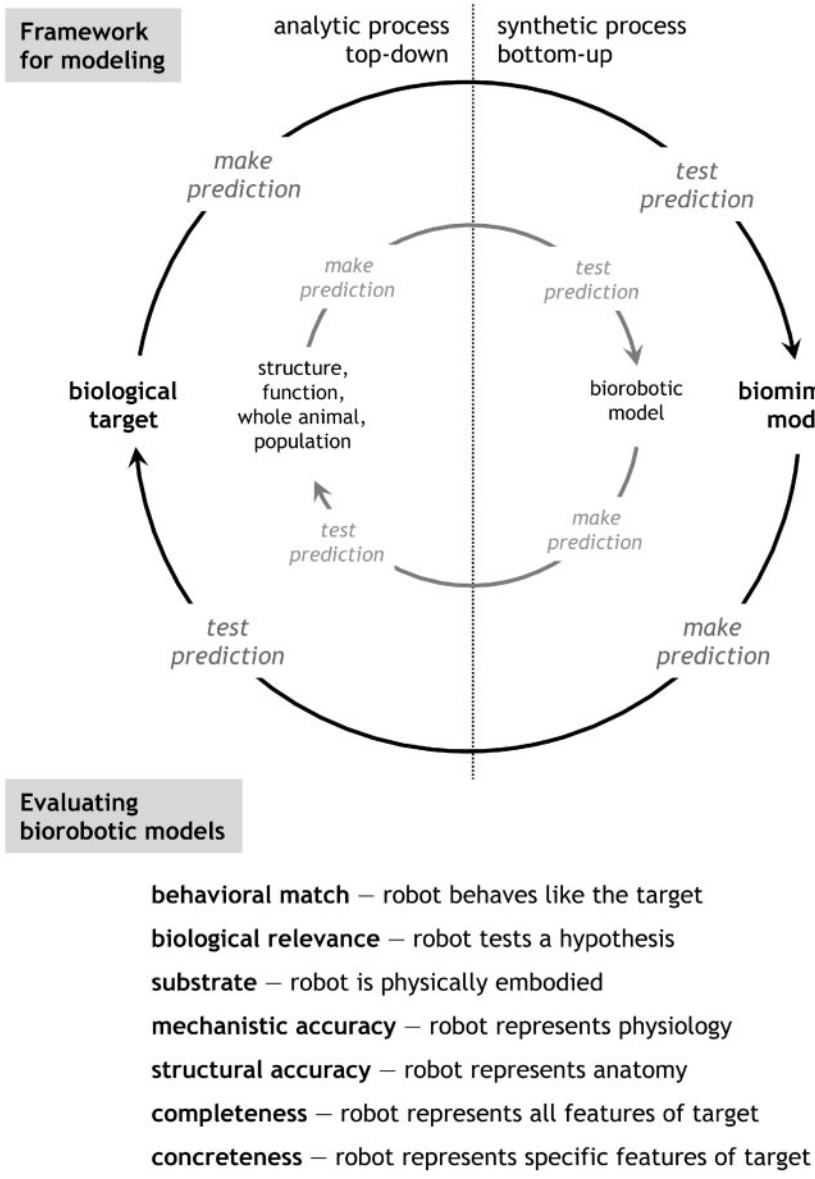

Fig. 1 Using biomimetic models to test biological hypotheses. Framework for modeling: in the most general sense (outer circle), the investigator selects a biological target and makes predictions about the mechanisms and/or structures that govern the target's operation. To test those predictions, the investigator builds a biomimetic model. The behavior of the model is usually compared to the behavior of the target to evaluate. For our work, we are interested in locomotion, and our biological targets include specific structures and functions of whole animals (middle circle). Our predictions, derived from the hypothesis that stiffness of the body is a key variable controlling swimming behavior, are tested by building a biomimetic vertebral column (BVC) that propels a biorobotic model. Evaluating models: while behavioral match is a frequent means of evaluating models, it is not the only one. For biorobotic models in particular, Webb (2001) offers seven dimensions by which models may be judged, requiring biorobots to show biological relevance and to be physically embodied rather than digitally simulated. Mechanistic and structural accuracy are two additional dimensions that we employ in the work presented here. Webb contends that it is the job of any model-builder to explicitly articulate and justify the dimensions that they use to evaluate.

is this: stiffness of the body in fish controls swimming behavior and stiffness of the body can, in turn, be altered by the morphology of the vertebral column. We use the word "control" in the context of control theory, where body stiffness is one of many possible causal agents that fish can manipulate to determine swimming behavior.

Following a review of biomimetics in fish-like robots (Long 2011), we use the term "biomimetic" to refer to engineered systems attempting to duplicate biological structures or functions; "bioinspired" refers to engineered systems that operate using a functional principle extracted from a biological system. When referring to "robot" or "biorobot",

we mean a physically embodied—not digitally simulated—electromechanical device that models the dynamic interaction of part, or all, of an animal with its environment.

Several lines of evidence support the hypothesis that body stiffness, measured here as the apparent material stiffness, E (in MPa), controls swimming behavior (Librizzi et al. 1999). By building a physics-based digital simulation of a swimming lamprey, complete with external fluid forces coupled to internal body forces, Tytell et al. (2010) showed that changes in body E modulate acceleration and average swimming speed, with a different optimum value for each metric. In self-propelled physical models of pumpkinseed sunfish, *Lepomis gibbosus*, McHenry et al. (1995) showed that swimming speed varies with changes in the models' E. Extrapolating from the passive body E of sunfish, McHenry et al. (1995) predicted that living sunfish would use their muscles during swimming to increase the apparent E of their body. Consistent with those predictions, correctly timed myomeric muscle activity tripled the body's E in whole-body-work-loop experiments on an eel, *Anguilla rostrata* (Long 1998). In the Atlantic hagfish, *Myxine glutinosa*, in which 75% of the body's passive E comes from the continuous notochord, the body's E increases, without muscular input, as the frequency of the cycle increases (Long et al. 2002). Thus, both active (muscular) and passive mechanisms are in place for fish to modulate their body E in response to the changing physical demands of different behaviors.

The passive E of the axial skeleton may be controlled, in part, by the number, size, and spacing of vertebrae. When artificial ring vertebrae were added to *ex vivo* notochords of *M. glutinosa*, the newly created vertebral columns increased their bending E in proportion to the number of vertebrae, N (Long et al. 2004). When an axial skeleton and its vertebrae are of fixed length, increasing N decreases the axial length of the invertebral joints. In most living fishes with vertebrae, lengths of the intervertebral joints are a fraction of the lengths of the vertebral centra, even though N itself is highly variable among species (Ward and Brainerd 2007). Increases in N are associated with greater curvature of the body during cruising (Long and Nipper 1996), tighter curvature during startle responses (Brainerd and Patek 1998), and elongated form of the body (Ward and Mehta 2010). In addition, N is correlated with differences in body shape and behavioral ecology (Mehta et al. 2010). In the Early Cambrian vertebrate *Haikouichthys*, vertebral centra are widely spaced, forming intervertebral joints longer than the vertebrae (Shu et al. 2003), creating a vertebral column roughly equivalent to that of biomimetic vertebral columns (BVCs) with $N = 4$–6.

We varied N to modulate E in the BVCs of our bioinspired robotic swimmer, MARMT (mobile autonomous robot for mechanical testing). A BVC, connected to MARMT's yaw-oscillating servo motor, flexes laterally, and, in so doing, transmits mechanical work from the motor to the propulsive caudal fin attached to its free end. The BVCs had a fixed overall length of 84 mm, had vertebrae of a fixed length of 5 mm, and varied in N from 0 to 11. In vertebrates, the ancestral state for axial skeletons is $N = 0$, which is a continuous notochord (Koob and Long 2000). When $N = 10$ or 11, the BVCs have intervertebral joints with axial lengths overlapping with the joint lengths measured in the vertebral columns of living sharks, both in absolute terms and relative to the length of the vertebrae (Porter et al. 2009). Not all of the BVC's we built match the spacing of the joints of known species, However, one of the useful features of biomimetic systems is that they can be manipulated to understand and predict the function of intermediate forms that are likely to be discovered in the fossil record.

We tested the hypothesis that the stiffness of the body in fish controls swimming behavior and stiffness of the body can, in turn, be altered by the morphology of the vertebral column. We also tested, as a secondary hypothesis, that an individual fish, with a fixed vertebral morphology, stiffens its vertebral column when it undulates at a higher frequency, f (Hz). This expectation is based on biomechanical data that show that E of *ex vivo* notochords and vertebral columns, tested in bending, increases as f increases (Long 1992; Long et al. 2002). Since f is under control of neural activation, we call f-mediated changes of E "activational control," in contrast to the "structural control" of E by way of N.

We tested the following predictions using BVC's with different values of N, undulated at different values of f, in dynamic bending tests (Predictions 1 and 2) and in a bioinspired swimmer, MARMT (Predictions 3 and 4):

(1) Structural control (N) of stiffness. Increasing the number of vertebrae, N, will increase the apparent storage modulus, E', and loss modulus, E'', of the BVC: $E', E'' = F(N)$, read as E' and E'' are some function, F, of N.

(2) Activational control (f, κ) of stiffness. Increasing the bending frequency, f (Hz), and bending curvature, κ (m^{-1}), will increase the E' and E'' of the BVC: $E', E'' = F(f, \kappa)$.

(3) Stiffness control (E', E'') of startle behavior. BVCs made stiffer by structural or activational control will increase the maximum acceleration, a_{max}, of MARMT during a startle response: $a_{max} = F(E', E'')$.

(4) Stiffness control (E', E'') of cruising behavior. BVCs made stiffer by structural or activational control will increase the average speed of MARMT, U, during steady forward cruising: $U = F(E', E'')$.

Methods

BVC

The biological target was the vertebral column of the spiny dogfish, *Squalus acanthias* (Fig. 2A). The vertebral column of *S. acanthias* is composed of cylindrical, amphicoelous, and mineralized vertebral centra that possess an intracentral canal through which a persistent notochord passes, connecting intervertebral capsules. Because the neural and hemal arches do not contribute to the compressive stiffness of the vertebral column in other sharks (Porter and Long 2010), we omitted these extra-central structures from the BVC.

With respect to the dimensions for evaluating models (Fig. 1), the BVC's were built with mechanistic and structural accuracy in mind. Mechanistic accuracy refers to the mechanical behavior of the BVC, measured by the apparent storage and loss moduli (E' and E'', respectively, in MPa) of the whole BVC under dynamic sinusoidal bending. Please note that the use of the term "apparent" here is meant to recognize that a composite structure, like a BVC, is composed of different materials, each with their own E' and E'' values.

BVC's were built in a manner identical with that used to make BVCs for evolving robots testing hypotheses about the selection pressures driving the

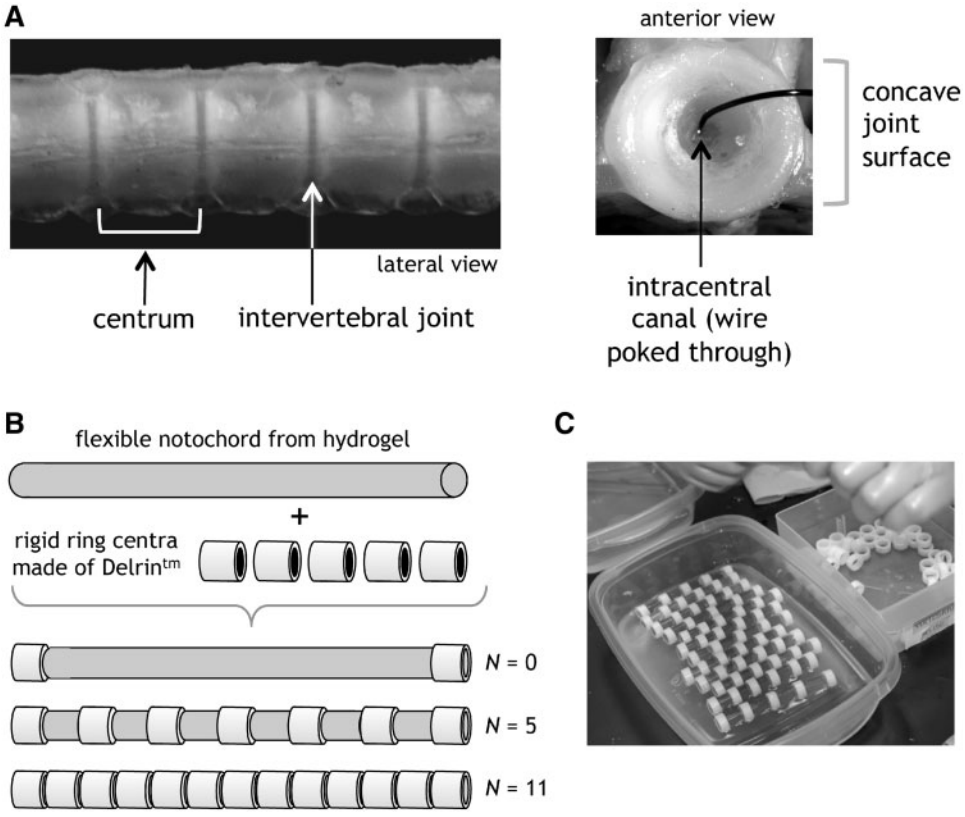

Fig. 2 Biomimetic vertebral columns (BVC) model the vertebral column of sharks. (**A**) The biological target is the vertebral column of the spiny dogfish, *S. acanthias*. The simple ring centra that make up the vertebral body possess an intercentral canal. (**B**) Biomimetic model: vertebral column with centra and canal. The BVCs are made from a flexible hydrogel molded from porcine gelatin crosslinked in 1.0% glutaraldehyde. The ring centra are made from rigid Delrin™, slid onto the hydrogel, and affixed with cyanoacrylic glue. The number of vertebrae, N, can be varied from 0 to 11. (**C**) Biomimetic vertebral column: assembly. BVCs with variable N are made for three purposes: (1) to characterize their variation in dynamic mechanical behavior under sinusoidal bending; (2) to test the hypothesis that increasing N alone will increase the apparent material stiffness, E (MPa), of the vertebral column; and (3) to test the hypothesis that increasing N and increasing E will create vertebral columns that enhance swimming behavior, all else being equal.

evolution of vertebrae (Doorly etal. 2009). A continuous and homogeneous "notochord" was first created from a hydrogel made of a 0.1 −g l^{-1} solution of gelatin (porcine skin, Type A; Sigma, St Louis, MO, USA) from powder dissolved in heated, distilled water. The gelatin solution was poured into and cooled in cylindrical molds that had a 1.0-cm inner diameter. To provide mechanical stability at room temperature and to increase stiffness, the hydrogels released from the molds were cross-linked in a solution of 2.5% phosphate-buffered glutaraldehyde for 1 h on a shaker table. After fixation and 24 h in a 20% EtOH storage solution, the diameter of the hydrogels had shrunk to an outer diameter of 0.8 cm. In a series of tests of aging, we concluded that hydrogels were stable in terms of size, mass, and mechanical properties from one to 5 days after fixation. All hydrogels were used within this 1–5 day window.

Hydrogels were inspected for damage; those undamaged were cut to 8.4 cm in length for standardization. To each end, a 5-mm-long vertebra was affixed using cyanoacrylate glue (Fig. 2B). These vertebra were machined from Delrin^{TM} (20% polyoxymethylene from DuPont Inc., USA), a rigid thermoplastic with *E*-values of ~3 GPa (Delrin Design Guide, Module III, from DuPont), making the vertebrae more than three orders of magnitude stiffer than the hydrogels used in this study. We do not know if this difference in *E* between the vertebrae and the intervertebral joints is biologically accurate, since relevant data in sharks have not been published. From blue marlin, *Makaira nigricans*, a bony fish, we know that isolated intervertebral joints have *E*-values, measured in bending, that range from 0.2 to 3 MPa (0.0002–0.003 GPa). For comparison, the vertebrae of sharks, composed of highly mineralized cartilage, have *E*-values in compression as high as 0.5 GPa, although this maximum varies widely among species (Porter et al. 2006).

The two vertebrae at the ends of the BVC were used as clamping sites for mechanical testing and for operation in the bioinspired robot. These vertebrae were not included in counts of the number of vertebrae, *N*, that characterized different kinds of BVC (Fig. 2B). The number of vertebrae, *N*, ranged from 0 to 11 producing 12 different kinds of BVC. The BVC with $N=0$ is analogous to a notochord; the BVCs with $N=10$ and 11 overlap, in terms of both the absolute and relative axial length of the intervertebral joints, with the vertebral column of *S. acanthias*. With $N=10$ and 11, the axial lengths of the intervertebral joints in the BVC were 1.1 and 0.5 mm, respectively. This compares to lengths of axial intervertebral joints that ranged from 0.4 to 1.5 mm (with vertebrae ranging from 4.4 to 7.3 mm in axial length) in the joints rostral to the caudal fin in a single fresh specimen of *S. acanthias* (for other species, see Porter et al. 2009).

Mechanical properties of the BVCs in bending

Three replicates of each of the 12 kinds of BVC were tested at 20°C at five different bending frequencies, f (Hz)—0.25, 0.50, 1.00, 1.50, and 2.00 Hz—at each of three different curvature amplitudes, κ (m^{-1})—1, 2, and 3 m^{-1}. Thus, each of the 36 BVCs was tested using 15 different mechanical inputs for a total of 540 mechanical tests.

For each test, two variables were measured, E' and E'' (see previous section for nomenclature). The E' was measured as the linear slope of the work loop of ten cycles of sinusoidal bending measured in terms of stress, σ (Pa), and strain, ε (non-dimensional). The σ was calculated from the following equation (Wainwright etal. 1976):

$$\sigma = \frac{Md}{2I} \quad (1)$$

where M (Nm) is the bending moment, d (m), is the diameter of the BVC, and I (m^4) is the second moment of area of the BVC. The M was calculated as the product of the moment arm, r (held constant at 0.06 m), and its normal force, F (N), delivered by the linear actuator of the testing machine (Tytron 250; MTS Systems, Eden Prairie, MN, USA) and measured by a calibrated ±25 N load cell (Fig. 3A).

The ε was calculated from the geometry of the bending rig, the specimen, and the instantaneous translation, x (m), of the MTS actuator (Fig. 3B):

$$\varepsilon = \frac{2\alpha(R - d/2)}{g} \quad (2)$$

where α is half of the angle corresponding to the specimen's arc length, R is the specimen's radius of curvature (m), d is the specimen's diameter (m), and g is the specimen's gage length (m), which was held constant at 0.084 m for all tests. The E'' was measured from the phase lag, δ (rad), between the σ and ε signals, where tan δ is the ratio of E'' to E'.

This method assumes that the specimen is undergoing pure bending, which was verified visually using video analysis of curvature. Note that κ is inversely proportional to the maximum R for any test. Measurements from the load cell and actuator displacement were sampled at 100 Hz. During testing,

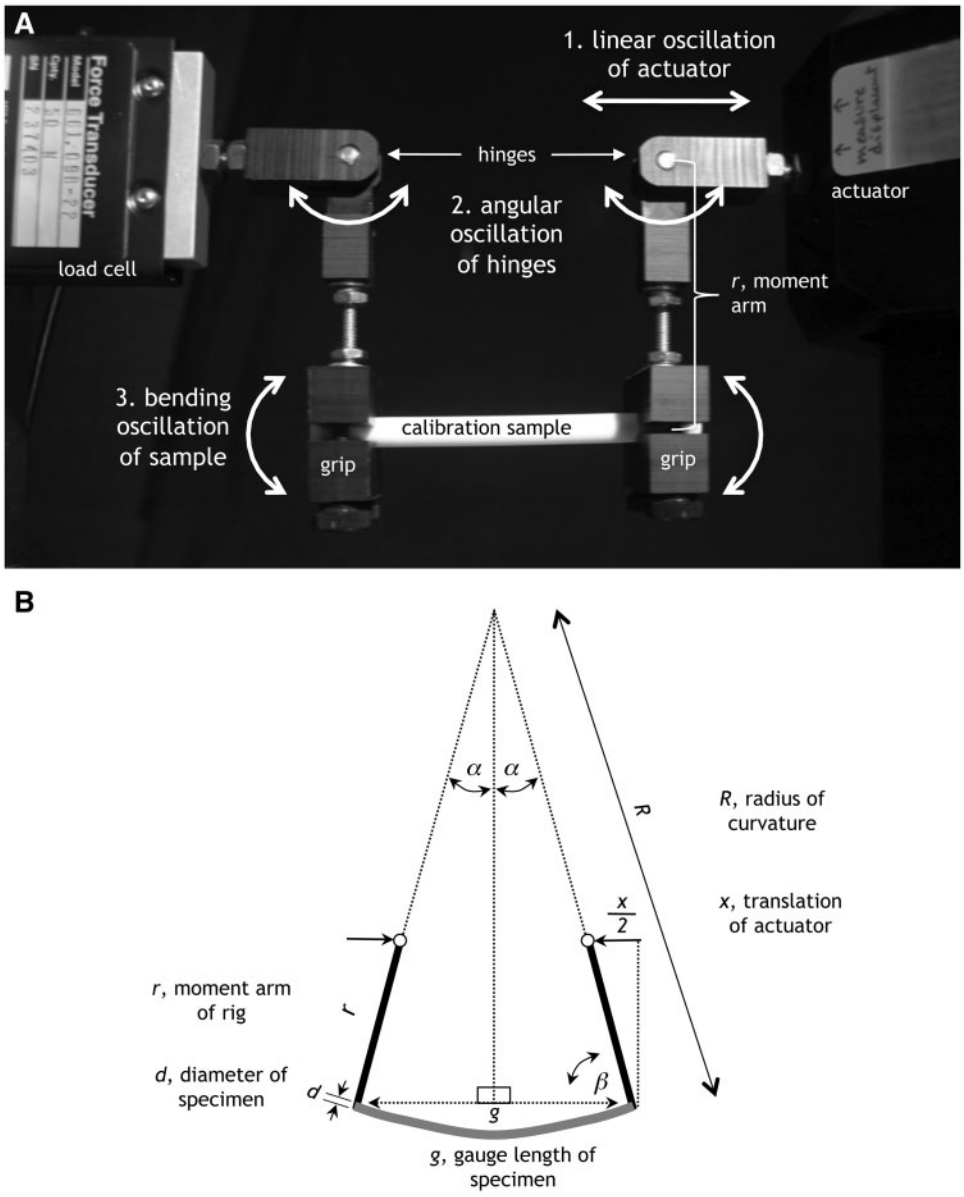

Fig. 3 Dynamic sinusoidal bending system. (**A**) When the linear actuator from the testing machine (MTS Tytron 250) oscillates at a set displacement amplitude and frequency, the hinges move closer and then farther apart. If the moment arms are both attached to a sample, here shown as a calibration sample, the linear oscillation of the actuator (1) will cause the moment arms to oscillate about the hinges (2) in anti-phase to each other. The simultaneous tilting of the moment arms imparts couples to the ends of the sample that cause the sample to oscillate in bending. With a moment arm, r, held constant at 6 cm, bending frequency, f (Hz), and curvature, κ (m^{-1}), are the variable inputs in this study. (**B**) Geometries and measurements used to calculate the strain of the specimen. See Equation (2) in the text.

each BVC was bathed in a 20% EtOH storage solution at room temperature.

To validate this procedure, we compared E' of BVC ($N=0$) measured in this study with the E' of BVC ($N=0$) produced in an identical manner for a different study (Long et al. 2006). The previous BVC were independently tested on a custom-built dynamic testing machine, which applied a single bending couple to the free end of a cantilevered BVC. The fixed end of the BVC was attached to a strain gage loaded in bending. For a κ of 1.71 m^{-1} at a f of 1.76 Hz, this cantilevered machine measured a single BVC's E' as 0.551 MPa. Using the Tytron 250 and custom bending rig of this study, a κ of 2.0 m^{-1}, and a f of 2.0 Hz, we measured the average of three BVC's E' as 0.580 MPa. The E'-values of the identical BVC's in the two different machines differed by 5.3%.

Bioinspired robot, MARMT

We built a bioinspired robot that could use (1) the BVC as its primary skeletal structure for propulsion and produce (2 *a*) startle responses and (2 *b*) cruising behavior. We modified the surface-swimming Tadro design (Long et al. 2006; Doorly et al. 2009) to build MARMT. Instead of Tadro's light and infrared sensors for inputs, MARMT was equipped with switches and potentiometers to allow investigators to quickly alter motor output without needing to manually reprogram the microcontroller onboard MARMT. The main hull of MARMT, a round plastic bowl, was 18-cm long at the waterline. MARMT's total submerged length was 38 cm TL from the bow to the distal tip of the caudal fin. A 9.6 V Ni-MH rechargeable battery pack powered the servo motor (JR Sport ST47BB Standard Ball-bearing). Motor commands to the servo were dictated by the microcontroller (MAKE microcontroller, Maker Media, O'Reilly Media, Sebastopol, CA, USA). The microcontroller received input from three potentiometers and four switches. The potentiometers allowed experimental control of tail-beat amplitude, tail center, and undulatory frequency. The four switches dictated power (off, on), behavior (startle, swim), direction of startle (left, right), and a switch to lock all inputs.

MARMT's software program, written in C, controlled the amplitude of the rotational yaw and the velocity of the servo motor that was mounted on the stern of the main hull and attached via a vertical shaft to the submerged BVC tail. The servo motor delivered an oscillating bending moment in the horizontal plane to the BVC tail. The BVC tail consisted of a BVC attached to an insert rostrally that was screwed into a slot on the shaft of the servo motor. Caudally, the BVC was attached to a rigid plastic caudal fin with a 2-cm trailing edge span, a 2.5-cm cord length, and a 30° flare from peduncle to trailing edge. Total length of the BVC tail was 11 cm from the servo shaft to the end of the caudal fin.

With respect to the dimensions for evaluating models (Fig. 1), MARMT was built with mechanistic accuracy in mind, the mechanism being swimming by using the body and the caudal fin. As occurs in fish, the startle response of MARMT consisted of a two-stroke turn from rest (Fig. 4). With the BVC tail straight, MARMT would swing the BVC tail to the left 90° in stage one and immediately swing the BVC tail back to the right 180° in stage two. Stage one produced yaw initially and stage two produced forward translation. MARMT was programmed to startle with the BVC moving at five different undulatory frequencies, $f(\mathrm{Hz}) = 0.25$, 0.50, 1.00, 1.50, and 2.00 Hz. For example, at $f = 0.25$ Hz, stage one and two occurred with periods of 2.0 and 4.0 s, respectively. At $f = 2.0$ Hz, stage one and two occurred with periods of 0.25 and 0.50 s, respectively. Steady undulatory cruising was also programmed as a series of sinusoidal oscillations, ±45°, of the servo motor at five different *f*: 0.25, 0.50, 1.00, 1.50, and 2.00 Hz.

Swimming performance of MARMT

During experiments, MARMT carried a three-axis wireless accelerometer (Wireless Dynamic Systems Sensor, Vernier Software & Technology, Beaverton, OR, USA) that measured translational and orthogonal components at a sampling rate of 500 Hz. The ventral surface of MARMT was also videotaped in a clear-bottomed tank. From the accelerometer and video, we measured three responses: (1) maximum composite acceleration in the horizontal plane, a_{max} (ms^{-2}); (2) average speed over one second, U (ms^{-1}); and (3) lateral amplitude of the tail, y (m). The a_{max} was determined by finding the maximum value of the vector sum of the two horizontal components of acceleration during a startle response. The U was calculated by taking the integral of the acceleration component in the axial direction over one second during MARMT's cruising. The y was measured from videotape as half of peak-to-trough excursion of the tip of the caudal fin.

MARMT was tested in a total of 360 trials of swimming performance. The BVC served as the fundamental experimental unit. Three of each kind of the 12 BVCs were made and turned into 36 BVC tails. Each of the BVC tails was tested in two behavioral categories, startle response and cruising. Within each kind of behavior, five different *f* were tested. Thus each BVC underwent ten trials (2×5); overall 36 BVCs underwent 360 trials. The order of the trials was randomized with respect to *N*, *f*, and behavior.

Statistical design

In testing the BVCs biomechanically and as part of MARMT's propulsive machinery, individual BVC were the equivalent of our experimental subjects. In mechanical tests, each BVC was tested at three κ conditions: 1, 2, and $3\,\mathrm{m}^{-1}$. Within each κ, the BVC was tested at five conditions of *f*: 0.25, 0.50, 1.00, 1.50, and 2.00 Hz. This totaled 15 separate tests for each BVC. Please note that this is not a simple repeated-measures design, since *N* varied across our subjects, by design. To account for repeated measures, we used the Bonferroni

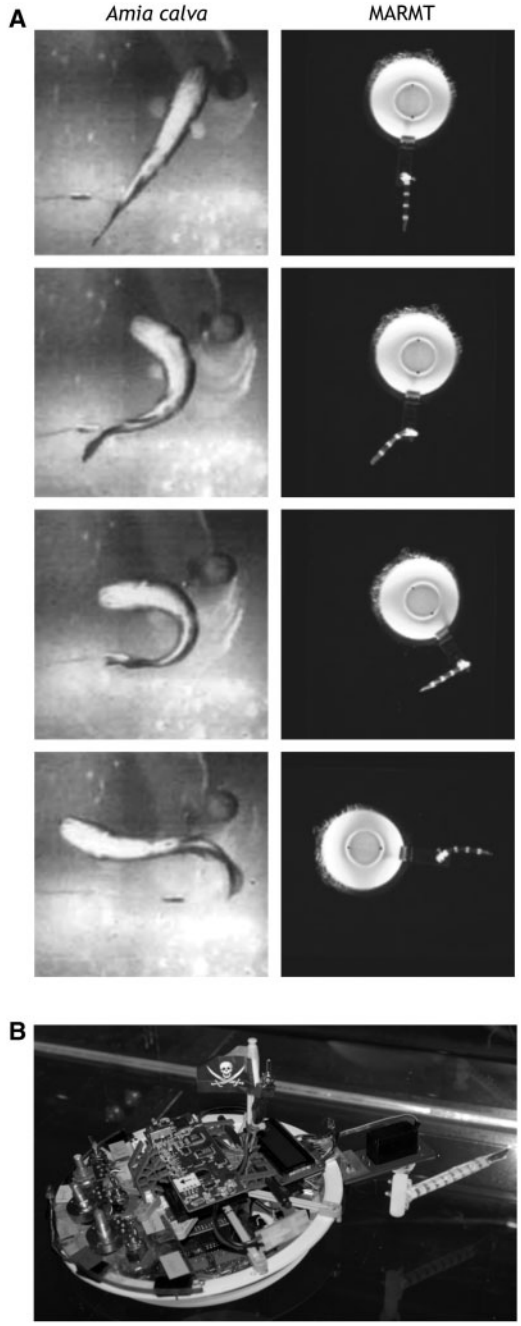

Fig. 4 The MARMT models turning during a startle-response in fish. (**A**) An 18-cm-long bowfin, *Amia calva*, accomplishes stages one and two of a startle-response within about 120 ms (Hale etal. 2002). At the maximal activation that we employed (cycle frequency, *f*, of 2.0 Hz), the MARMT (18 cm at the waterline; 38 cm TL submerged from bow to distal tip of caudal fin) accomplishes stages one and two of a startle-response turn in a minimum time of 750 ms, with stage one complete in 250 ms. While MARMT turns much more slowly than does *Amia*, note that the kinematic outputs are otherwise similar, with both turning about 90° to the right using a half tailbeat to the left followed by a tailbeat to the right. Ventral views. (**B**) MARMT carries a three-axis accelerometer (under the flag) and a microcontroller that carries out the motor commands for startle-response turns or cruising (data not shown). Note that MARMT swims at the surface and is propelled by its fully submerged BVC and associated caudal fin. A single servo motor inputs a rostral bending couple to the BVC + caudal fin.

correction; with an $\alpha = 0.05$, all statistical tests had to achieve $P < 0.0033$ to be considered significant. In total, 36 BVC were tested.

For the swimming trials with MARMT, each BVC utilized two behaviors and, in each behavior, five f conditions: 0.25, 0.50, 1.00, 1.50, and 2.00 Hz, for a total of 10 tests. To account for repeated measures in swimming trials, we used the Bonferroni correction; with an $\alpha = 0.05$, all statistical tests had to achieve $P < 0.005$ to be considered significant. Fully factorial ANOVAs were run using JMP 8.0 software. The factors N, f, and k were all fixed effects. In total 36 BVC were tested.

Results

Mechanical properties of the BVCs in bending

All statistical results are reported after Bonferroni correction. For example, if a significance of $P < 0.05$ is reported, then the test is significant at that level. To determine the corrected P-value, which is reported here, we took the raw P-value, which is not reported, and divided it by the number of repeated measures (see 'Methods' section). A fully-factorial ANOVA with the storage modulus, E', as the response variable was significant (overall $P < 0.0001$, adjusted $r^2 = 0.900$, $F = 964.14$, $n = 540$). All the main effects positively and significantly related to E' (Fig. 5): number of vertebrae, N ($P < 0.0001$), amplitude of the curvature, κ ($P < 0.0001$), and bending frequency, f ($P < 0.0001$). Three of the four interaction terms were significant: $N \times \kappa$ ($P < 0.0001$), $N \times f$ ($P < 0.05$), and $\kappa \times f$ ($P < 0.0001$).

A fully-factorial ANOVA with the loss modulus, E'', as the response variable was significant (overall $P < 0.0001$, adjusted $r^2 = 0.676$, $F = 161.54$, $n = 540$). All the main effects were significantly related to E'' (Fig. 6): N ($P < 0.0001$), κ ($P < 0.0001$), and f ($P < 0.0001$). The N and κ were positively related to E'' and f was negatively related. Two of the four interaction terms were significant: $N \times \kappa$ ($P < 0.0001$) and $\kappa \times f$ ($P < 0.0001$).

These results support Predictions 1 and 2 (see 'Introduction' section), that the E' and E'' of the vertebral column are under structural (N) and activational (f, κ) control.

Swimming performance of MARMT

For startle responses, a fully-factorial ANOVA with the peak acceleration, a_{max}, as the response variable was significant (overall $P < 0.0001$, adjusted $r^2 = 0.761$, $F = 191.21$, $n = 180$). Both main effects were positively and significantly related to a_{max}

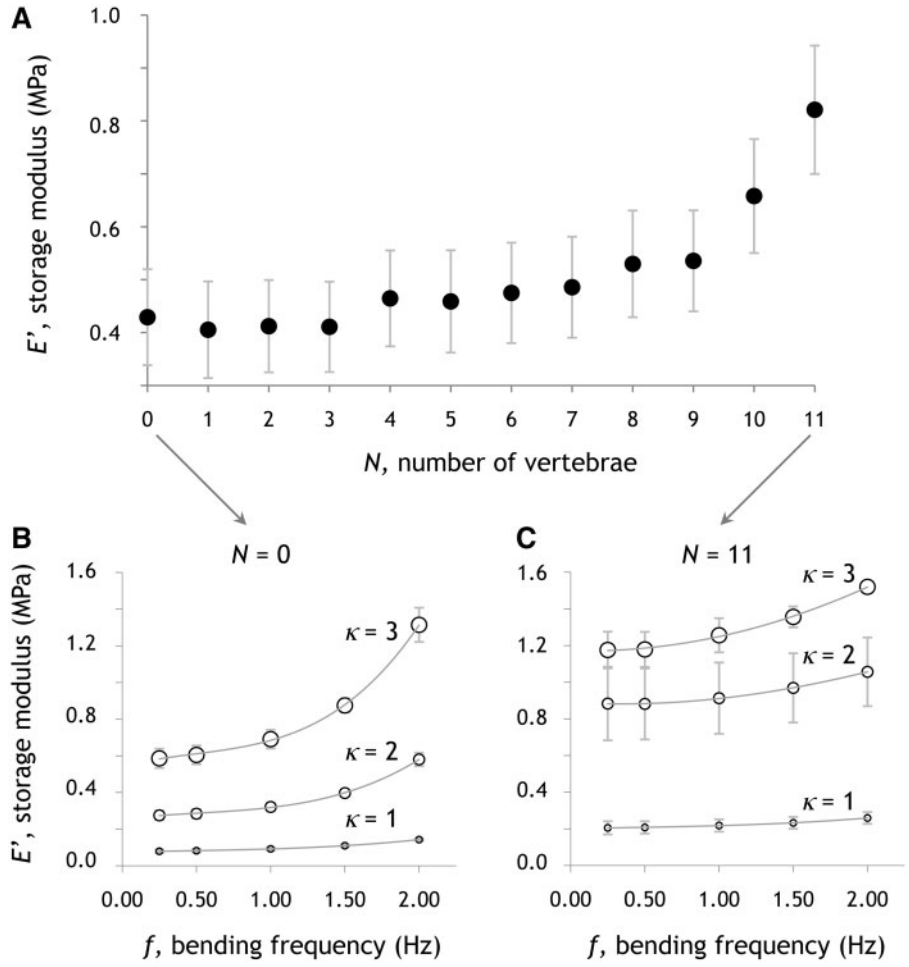

Fig. 5 Mechanical behavior of biomimetic vertebral columns (BVC) during sinusoidal bending, as measured by the storage modulus, E'. (**A**) E' increases as the number of vertebrae, N, increase. Filled circles represent means (pooled over bending frequency, f, and bending curvature, κ). Error bars represent one standard error of the mean. (**B** and **C**) The only statistically significant interactions ($P<0.001$) are $N \times \kappa$, $N \times f$, and $\kappa \times f$. The $N \times \kappa$ interaction can be seen as the increase in the magnitude of the response to increasing κ from B ($N=0$) to C ($N=11$). The $N \times f$ interaction can be seen as the greater slopes of the regression lines in B ($N=0$) compared to those in C ($N=11$). The $\kappa \times f$ interaction can be seen as the increase in slopes as κ increases. Open circles represent means (three replicate BVCs). Error bars represent one standard error of the mean. In total, these data represent 540 tests of BVCs with 12 different numbers of vertebrae, each tested at five different values of f, and three values of κ. All three main effects, N, f, and κ, are statistically significant ($P<0.001$).

(Fig. 7): N ($P<0.0001$) and f ($P<0.0001$). The $N \times f$ interaction was also significant ($P<0.0001$).

For cruising, a fully-factorial ANOVA with the mean speed, U, as the response variable was significant (overall $P<0.0001$, adjusted $r^2=0.827$, $F=282.21$, $n=180$). Both main effects were positively and significantly related to U (Fig. 8): N ($P<0.0001$) and f ($P<0.0001$). The $N \times f$ interaction was also significant ($P<0.0001$).

For startle responses, neither the whole ANOVA nor any of the effects or interactions were significantly related to lateral amplitude of the tail, y. The mean y was $0.119\,\text{m} \pm 0.0023$ (one standard error; $n=180$). The same was true for cruising, with a mean y of $0.113\,\text{m} \pm 0.0022$.

These results support Predictions 3 and 4 (see 'Introduction' section), that a_{max} and U of the swimming MARMT can be altered by changes in the E' and E'' of the BVCs. The connection between stiffness (E', E'') and swimming performance is described in the next section.

Integrating the function of BVC and the swimming of MARMT

Because E', E'', a_{max}, and U are all functions of N, N can be used to build a mathematical relation between mechanical properties and swimming behaviors (Fig. 9). In regressions of the grand means of swimming behavior on the grand means of mechanical properties, N is parameterized, increasing in the

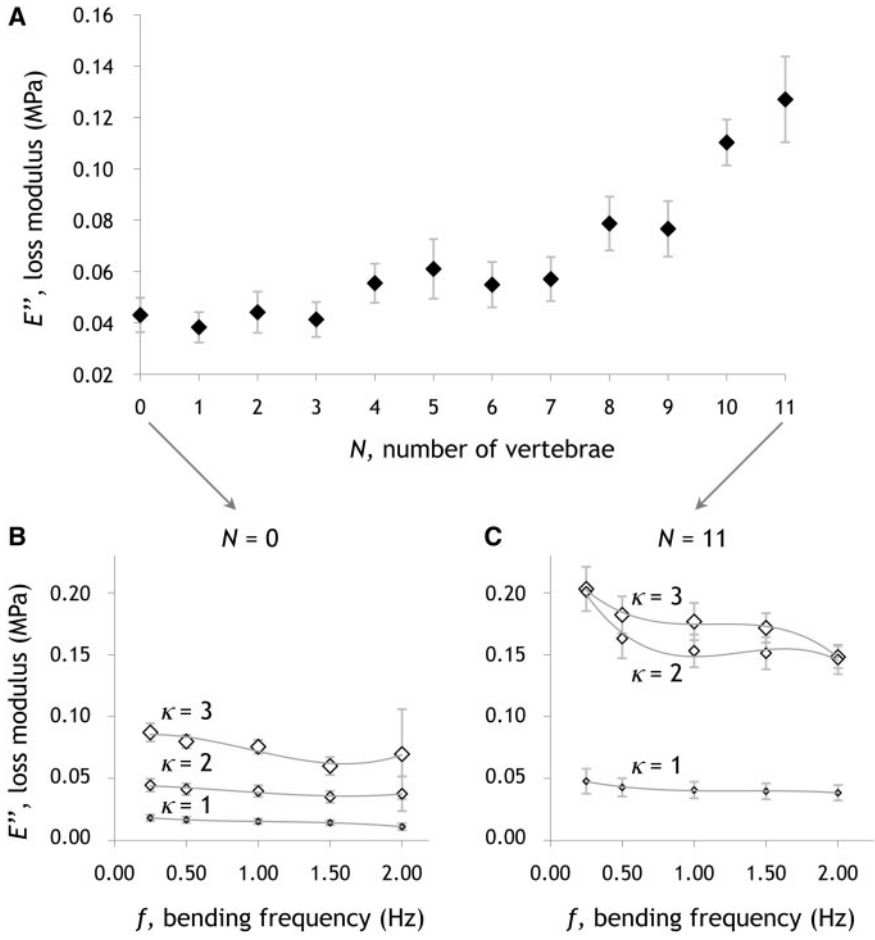

Fig. 6 Mechanical behavior of biomimetic vertebral columns (BVC) during sinusoidal bending, as measured by the storage modulus, E''. (**A**) E'' increases as the number of vertebrae, N, increase. Filled diamonds represent means (pooled over bending frequency, f, and bending curvature, κ). Error bars represent one standard error of the mean. (**B** and **C**) The only statistically significant interactions ($P<0.001$) are $N \times \kappa$ and $\kappa \times f$. The $N \times \kappa$ interaction can be seen as the difference in the magnitude of the response to increasing κ from $N=0$ to $N=11$. The $\kappa \times f$ interaction can be seen as the difference in slopes as κ increases. Open diamonds represent means (three replicate BVCs). Error bars represent one standard error of the mean. In total, these data represent 540 tests of BVCs with 12 different numbers of vertebrae, each tested at five different values of f, and three values of κ. All three main effects, N, f, and κ, are statistically significant ($P<0.001$).

positive direction along the following regression lines:

$$a_{\max} = 0.107 + 0.611E' \quad (3),$$

where $P=0.0002$, adjusted $r^2=0.748$, $F=33.73$, and $n=12$; and

$$U = -0.0079 + 0.3016E' - 0.6748(E')^2 \quad (4)$$

where $P=0.0023$, adjusted $r^2=0.563$, $F=15.15$, and $n=12$; and

$$a_{\max} = 0.238 + 2.724E'' \quad (5)$$

where $P<0.0001$, adjusted $r^2=0.796$, $F=43.90$, and $n=12$; and

$$U = 0.0685 + 1.1516E'' - 11.3494(E'')^2 \quad (6)$$

where $P<0.0013$, adjusted $r^2=0.723$, $F=15.37$, and $n=12$. Both E' and E'' in Equations 3–6 are in units of MPa. Second-order polynomials were used only when the second-order term had an effect significance of $P<0.10$.

Discussion

Biomimetic structures built as models of specific biological systems can be used to test biological hypotheses (Fig. 1). Those biomimetic models provide relevant tests of biological predictions if they operate under physical conditions that closely resemble those seen in the targeted biological system. Appropriate physical conditions for animal behaviors that involve movement can be achieved with physically embodied, self-propelled biorobots. Using this general approach, which is inspired by the biorobotic paradigm (Webb 2001, 2006; Webb and Consi 2001), robotic modeling in biomechanics

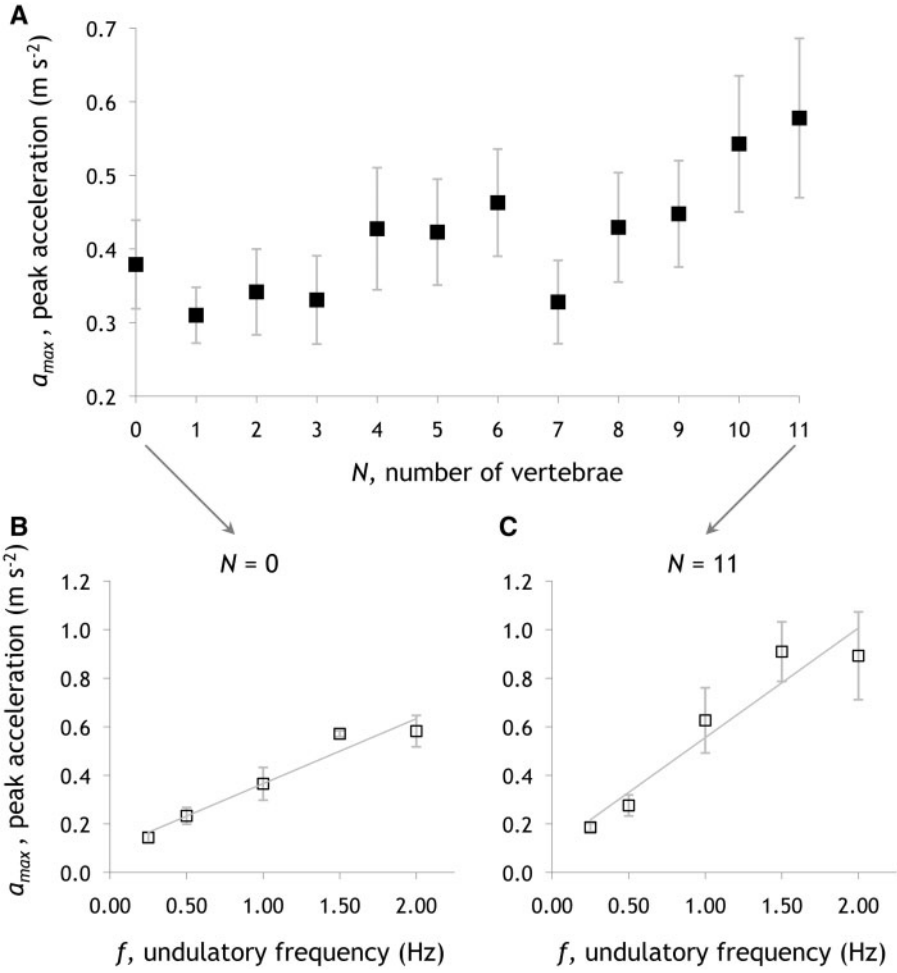

Fig. 7 Peak acceleration of MARMT during startle behavior. (**A**) The peak acceleration, a_{max}, increases as the number of vertebrae, *N*, increase. Filled squares represent means (pooled over undulatory frequency, *f*). Error bars represent one standard error of the mean. (**B** and **C**) The significant $N \times f$ interaction is shown by the difference in slopes in the linear regression for $N = 0$ (slope = 0.268) and for $N = 11$ (slope = 0.451). Open squares represent means (three replicate tails). Error bars represent one standard error of the mean. In total, these data represent 180 trials of MARMT propelled by BVCs with 12 different numbers of vertebrae, three replicates of each, at five different *f*.

(McHenry et al. 1995; Lauder and Madden 2006; Lauder et al. 2007), and biomimetic robotics (Fish 2006; Long 2007), we tested the hypothesis that stiffness of the body controls swimming behavior. This hypothesis was robustly supported by testing a range of BVCs acting as undulatory propellers in a bioinspired robot, MARMT.

Testing the predictions

The structural–control prediction—that the number of vertebrae, *N*, increases the apparent storage modulus, E', and loss modulus, E'', of the BVC—was supported by results from sinusoidal mechanical tests (Figs. 5A and 6A). Moreover, while we see a gradual increase in both E' and E'' from $N = 0$–9, both properties increase abruptly at the transition from $N = 9$–10. We suspect that this increase in the rate at which stiffness increases is caused by adjacent vertebrae being close enough that they abut on the concave side of a bend, as seen in close-ups of the BVC during the fastest startle responses (Fig. 10).

We explored only one parameter in vertebral morphospace: *N*. Since we held the length of the vertebral column constant, as *N* increased, the axial length of the intervertebral joints (IVJ) decreased. With an anatomical region of the vertebral column, fish increase *N* by decreasing the axial length of the centra (Ward and Brainerd 2007; Ward and Mehta 2010). Axial length of the IVJs may be constant, increase, decrease, or some mix of the three across an entire column, as seen in sharks (Porter et al. 2009). Most fish elongate their bodies by increasing *N* (Ward and Brainerd 2007). Vertebrae may also change shape, as measured by the ratio of centrum

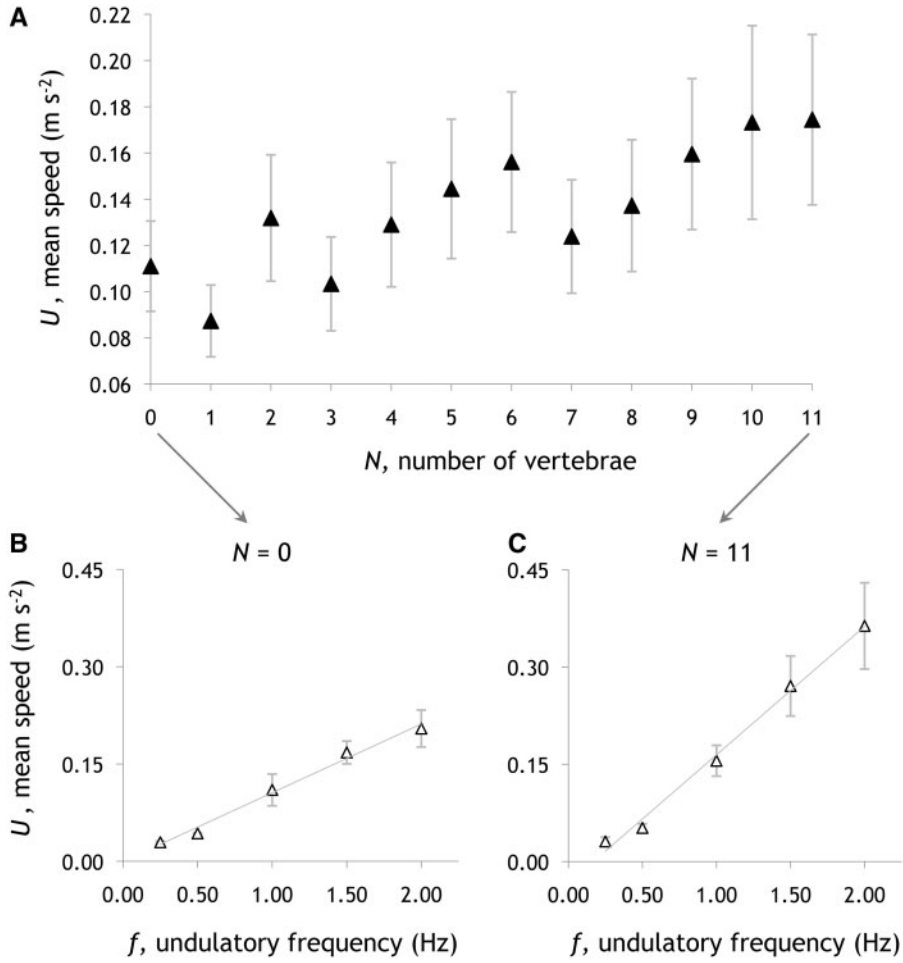

Fig. 8 Mean speed of MARMT during cruising behavior. (**A**) The mean speed, U, increases as the number of vertebrae, N, increase. Filled triangles represent means (pooled over undulatory frequency, f). Error bars represent one standard error of the mean. (**B** and **C**) The significant N-by-f interaction is shown by the difference in slopes in the linear regression for $N = 0$ (slope = 0.106) and for $N = 11$ (slope = 0.198). Open triangles represent means (three replicate tails). Error bars represent one standard error of the mean. In total, these data represent 180 trials of MARMT propelled by BVCs with 12 different numbers of vertebrae, three replicates of each, at five different f.

length to width, among species (Ward and Brainerd 2007; Porter et al. 2009; Mehta et al. 2010). While vertebral morphospace is clearly more complicated than the simple change in N we have modeled, the functional importance of N-mediated changes in axial length of the IVJs has clear mechanical consequences on E' and E''.

The activational-control prediction—that increasing the bending frequency, f (Hz), and bending curvature, κ (m^{-1}) increases the E' and E'' of the BVC—was also supported by results from sinusoidal mechanical tests (Figs. 5B and C and 6B and C). Of particular importance here are the significant interaction terms. The interactions $N \times \kappa$, $N \times f$, both significant for E', show a clear functional linkage between structural-control and activational-control. Structure and activation are not independent mechanisms. As N increases, the effect of increasing κ expands (Fig. 5B) while the effect of increasing f compresses (Fig. 5C). Only the $N \times \kappa$ interaction is significant for E'', with E'' increasing at a much faster rate with increasing κ at higher values of N.

Because E'' is proportional to the elastic energy lost during bending, which can be thought of as the mechanical cost of bending, this indicates a functional trade-off for the control of stiffness: if high N is chosen to increase E', mechanical costs will also increase because of an increasing E'' (Summers and Long 2006). This trade-off may explain why populations of evolving robots initially increase N but then reach an equilibrium value, with a population mean of $N = 5.7$, well below that predicted based on maximizing E' (Doorly et al. 2009). An open question is why living species of sharks have evolved vertebral

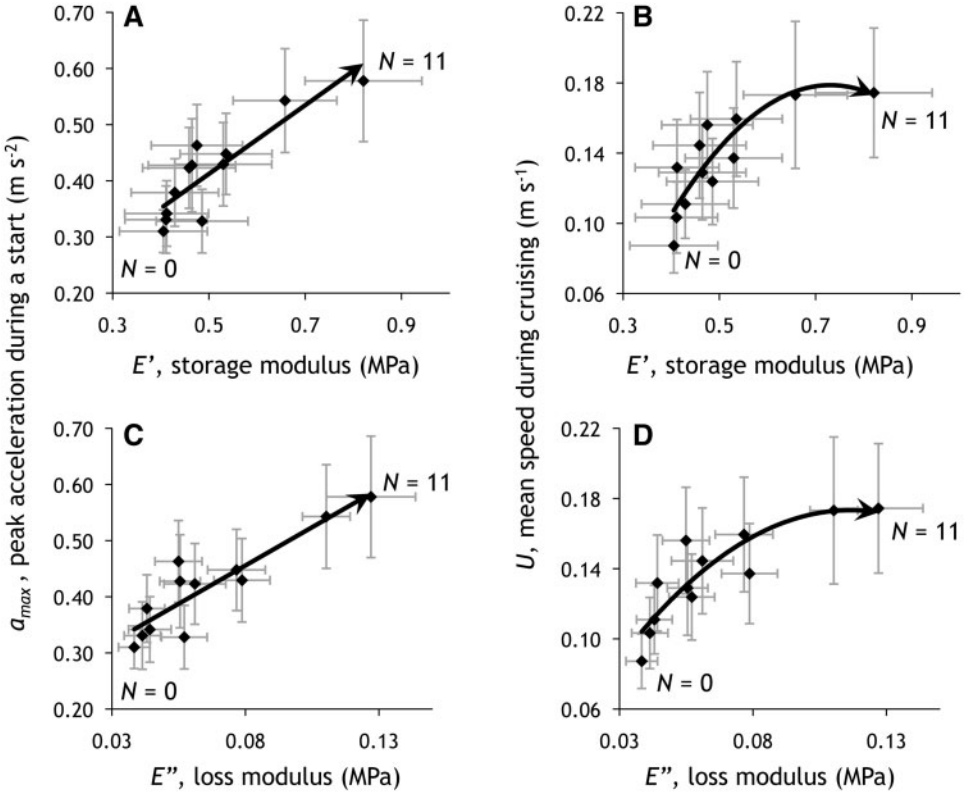

Fig. 9 The morphology and stiffness of biomimetic vertebral columns (BVC) modulate the swimming behavior of MARMT. Changes in MARMT's swimming behavior, as measured by peak acceleration, a_{max}, during a start and mean speed, U, during cruising, are caused by changes in the mechanical properties of the BVC. Changes in the BVC's mechanical properties, in turn, are caused by changes in the number of vertebrae, N. In mathematical terms, N is parameterized here within the equations that relate behavior to mechanical properties, as indicated by the arrow on the regression line and the labeling of low ($N=0$) to high ($N=11$) values on the line (see Equations [7–10] for parametric form). For a_{max}, linear regressions describe the E' and E'' ($r^2=0.771$ and 0.815, respectively). For U, second-order polynomials describe the relation with E' and E'' ($r^2=0.741$ and 0.774, respectively). Each point represents the mean value of 15 trials for acceleration and speed (pooled across f) and 45 tests for BVC's (pooled across κ and f). Error bars represent one standard error of the mean.

columns with intervertebral joint/vertebrae length proportions that match the BVC's proportions when $N=10$ and 11.

The stiffness-control prediction for acceleration, a_{max}—that BVCs made stiffer by structural or activational control will increase a_{max} of MARMT during a startle response—was supported by results from the robotiic experiments (Fig. 7). In terms of structural control, increases in N increased a_{max} (Fig. 7A). In terms of activational control, increases in f also increased a_{max} (Fig. 7B and C). With the swimming of MARMT, we see the same significant interaction, $N \times f$ that for the BVC alone linked the two structural and activational controls. At the highest values of N, the effect of increasing f on a_{max} is greater than at the lower values of N. Thus, any organic or robotic agent is likely to have greater behavioral range, measured in terms of a_{max}, if it has a greater N in its propulsive tail but, as mentioned above, that increased range comes with a mechanical cost.

The stiffness-control prediction for mean speed, U—that BVCs made stiffer by structural or activational control will increase U of MARMT during cruising—was supported by results from the robotic experiments (Fig. 8). We see the identical pattern for U that we saw for a_{max}. MARMT's cruising speed increases with increasing N and f, and at higher values of N, U increases more rapidly as f increases (Fig. 8B and C). Once again, without considering mechanical trade-offs, it would appear that more N gives the organic or robotic agent more behavioral scope.

Summarizing the structural control of the BVC and MARMT

One way to model the functional integration of morphology, stiffness, and behavior is to link all three mathematically (Fig. 9). If we define the system parametrically, we can set N as the free parameter such

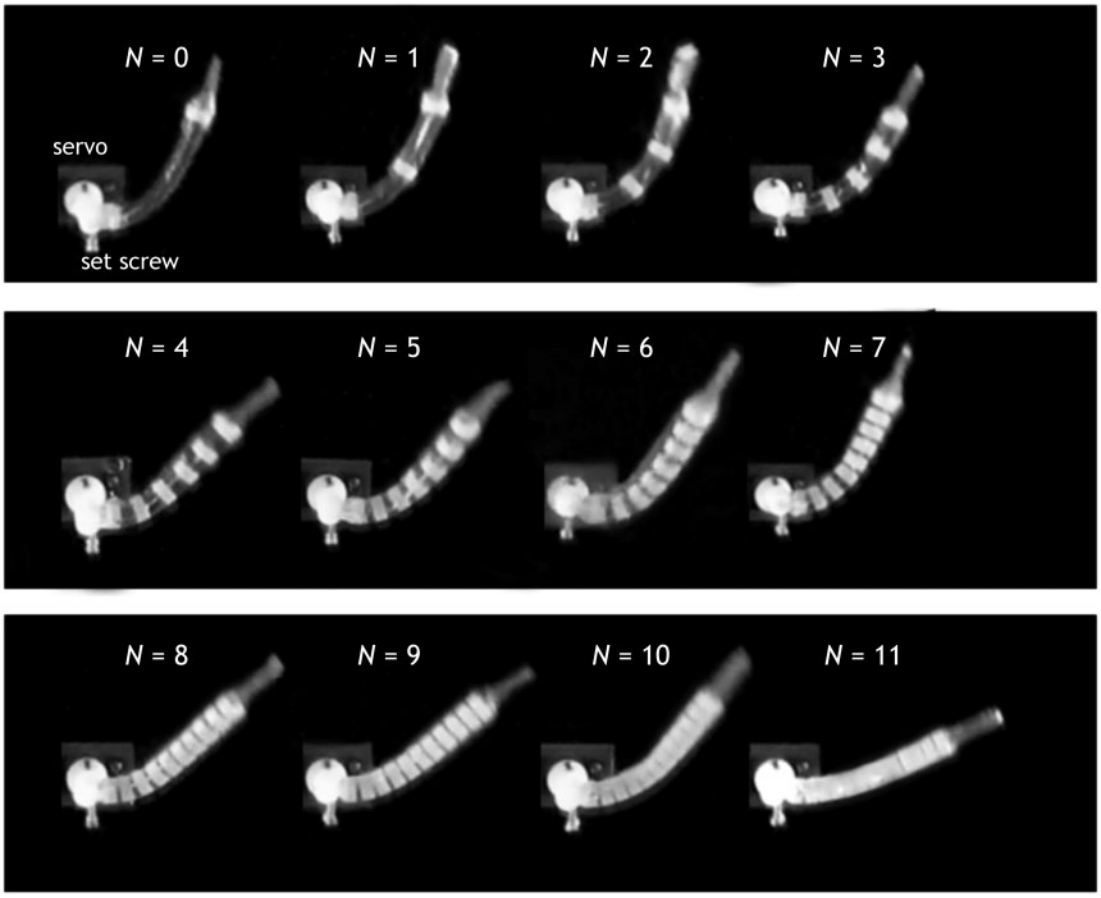

Fig. 10 Biomimetic vertebral columns (BVC) in action. BVCs with varying number of vertebrae, *N*, behave differently as propulsors of MARMT with the same activation parameters. In the startle-response behavior of MARMT shown here, the BVCs are activated identically by the servo motor at a cycle frequency, *f*, of 2.0 Hz (0.25 s for stage 1; 0.50 s for stage 2). At the middle of stage 2, shown here from the ventral perspective, the BVCs' curvature decreases as *N* increases. At $N = 9$ adjacent vertebrae begin to abut on the concave lateral surface towards the BVCs rostral end (to the left). Vertebrae abut almost completely at $N = 11$, when the lengths of the intervertebral joints are the shortest. All images are standardized in the activation cycle by the position of the set screw on the transmission shaft relative to the servo motor. Slight variations in position are due to temporal aliasing of the 30 Hz video.

that the entire BVC–MARMT system can be summarized in the following four equations:

$$E'(N) = 0.291 + 0.0284N + 0.00501N^2 \left(\text{adjusted } r^2 = 0.894\right) \quad (7)$$

$$E''(N) = 0.0611 + 0.00693N + 0.000956N^2 \left(\text{adjusted } r^2 = 0.919\right) \quad (8)$$

$$a_{\max}(N) = 0.316 + 0.0184N \left(\text{adjusted } r^2 = 0.574\right) \quad (9)$$

$$U(N) = 0.0991 + 0.00640N \left(\text{adjusted} r^2 = 0.689\right) \quad (10)$$

where E' and E'' are in units of MPa, data are pooled by f and κ, and we use the same rule about the order of polynomials in regressions that we followed in Equations (4–6) (see 'Results' section). Those four equations can be paired to produce the four different parametric paths described in Equations (4–6) and shown in Fig. 9. Along each path N increases from 0 to 11, and, in so doing, can be thought of as increasing both of its response variables. More accurately, as N increases, all four equations simultaneously increase their responses.

New predictions for swimming fish

The promise of this biomimetic–biorobotics approach is 2-fold (Fig. 1): (1) to test biological hypotheses using the model system, as seen above, and (2) to generate new predictions, based on the behavior of the model system that can be tested in turn by examining the biological target. Here, we present several new predictions about the vertebral

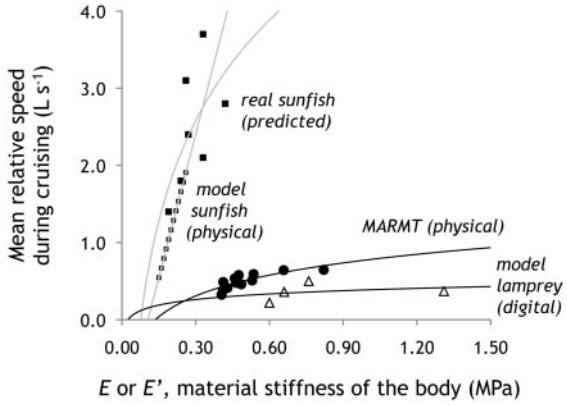

Fig. 11 Behavioral match of MARMT to other undulatory swimmers. In terms of mean relative swimming speed, where L is the body length, and material stiffness of the body, measured as either the complex or storage modulus, E or E', respectively, MARMT swims more like a digitally modeled lamprey (Tytell et al. 2010) than a pumpkinseed sunfish or a physically-modeled sunfish (McHenry et al. 1995). All lines are logarithmic regressions. All regressions extrapolate back to similar low values of E for a mean relative speed of 0. In all cases, note that increasing stiffness of the body increases the swimming speed.

columns and swimming behaviors of fishes that were generated from the BVC–MARMT system:

(1) Amplification of stiffness, E' and E'', by vertebral abutment. Vertebrae, by virtue of having greater stiffness than their intervertebral joints, amplify stiffness at high curvatures, when rims of adjacent vertebrae abut. This physical interaction is seen in the BVCs with the highest N (10 and 11) during the fastest startle responses (Fig. 10). A corollary prediction is that abutment of vertebral rims causes the neutral zone of bending, a region of zero body stiffness with respect to body curvature, to quickly make a transition to a region of elastic resistance in longnose gar, *Lepisosteus osseus* (Long et al. 1996). A second corollary prediction is that continuous notochords and vertebral columns with intervertebral joints of high axial length, equivalent to $N = 1$–9 in our BVC, do not show amplification of stiffness at high curvatures (compare Fig. 5B with C).

This prediction can be tested by measuring strain of the intervertebral joints and vertebral centra directly during dynamic bending. Instead of inferring strain from system and sample geometry (Fig. 3B), strain of individual joints and centra can be measured directly using video markers or ultrasonic transceivers.

(2) Limit to the curvature of the vertebral column, κ, by vertebral abutment. At the smallest lengths of axial joint, the abutment of centra not only amplifies E' and E'' (see Prediction 1), but also limits the curvature, κ, of the vertebral column (Fig. 10). If we assume that the intervertebral joints bend about their mid-lateral axis, then the angle of abutment—the limit to curvature of the joint—is a function of the axial length of the intervertebral joint and the transverse width of the adjoining centrum, its diameter in the case when it is round. Another assumption is that the centra have much greater stiffness than the intervertebral joints, such that the joints undergo most of the strain incurred during bending. Vertebral abutment may explain the limits to intervertebral joint angles measured during startle responses in tetraodontiform fishes (Brainerd and Patek 1998), limits to postural reconfiguration in general (Long etal. 2010), and the correlation of transverse width and intervertebral joint length with body curvature during turning in sharks (Porter etal. 2009).

Since this prediction involves physiological limits, it needs to be tested *invivo*. Those κ limits can be predicted specifically using data from mechanical testing (Prediction 1) or from morphometrics. *Invivo* testing of the predictions could involve direct imaging of the adjacent vertebral rims during swimming. A method for doing this has been developed using a 3D X-ray technique coupled with 3D morphology (Nowroozi and Brainerd 2010).

(3) Activational control of stiffness of the body will differ in species with notochords and species with vertebral columns. Because of the mechanical interaction of N with κ and with f (compare Fig. 5B and C), we predict that fish with notochords will vary f to modulate body stiffness while fish with vertebral columns will vary κ.

The problem with testing this prediction in swimming fish is finding a way to measure stiffness of the axial skeleton *invivo*. Appropriate methodology needs to be invented. Possible pathways include finding ways to measure changes in ultrasonic time of flight or changes in the transmission high-frequency pressure waveform across tissues that are changing in stiffness.

Evaluating BVC and MARMT as models of biological targets

Is a model a good representation of the biological target? In our case, is the BVC model a good representation of a biological vertebral column? Is the

MARMT model a good representation of a swimming fish? The answers to these questions depend on the intent of the investigators. Our intent, in the case of the BVC, was to model structural changes in the vertebral column, and to understand how those structural changes controlled stiffness and, in turn, swimming behavior. In terms of the evaluation scheme presented, and given that we took physical embodiment and biological relevance as givens in the biorobotic framework, the dimension upon which we focused was that of structural accuracy (Fig. 1).

When we designed the BVC, we attempted to model the jointed anatomy of the vertebral column of *S. acanthias*. Clearly, however, the BVC's ring centra are not as structurally complex as the biconic amphicoelous vertebrae of *S. acanthias* (Fig. 2A). While both have a continuous notochordal strand, the BVC's intracentral canal is too large, and the hydrogel lacks any of the cells or lacunae associated with intervertebral capsules (Symmons 1979; Schmitz 1995; Grotmol et al. 2005). Also, we kept the length of the vertebral column constant while altering the number of vertebrae, even though both features vary in fishes (Ward and Mehta 2010). Perhaps most importantly, the BVC lacks intervertebral ligaments that connect the rims of adjacent vertebrae (Symmons 1979). The best that can be said about the BVCs structural accuracy is that it is high only in building intervertebral joints of axial length close to that seen in sharks (see 'Results' section). To be fair, though, we did not intend, for this first BVC model, to include multiple structural levels.

Given the BVC's structural inaccuracy on many levels, it was encouraging to see good mechanical accuracy in terms of the magnitude of E' and its response to increases in f and κ. In terms of magnitude, E' of the BVC with $N = 11$, which overlaps vertebral column structure with *S. acanthias*, ranges from ~0.2–1.5 MPa (Fig. 5C). This range overlaps with the range of *E*-values measured under sinusoidal bending in the notochord of white sturgeons, *Acipenser transmontanus* (Long 1995), the intervertebral joints of blue marlins, *Makaira nigricans* (Long 1992), and the intervertebral joints of saddleback dolphins, *Delphinus delphis* (Long et al. 1997).

Our intent in building the self-propelled biorobot MARMT was to match the undulatory kinematics of fish performing (1) the vertebrate startle response and (2) steady cruising using the body and caudal fin. Before comparing kinematics, it's important to note that we recognize that MARMT's circular body is large relative to its propulsive tail; the closest living analogs are the electric rays (Krishnamurthy et al. 2010). Also MARMT swims with its body floating on the surface and its tail submerged, like an outboard motor on a dinghy rather than a fish underwater. Finally, MARMT actuates the BVC with a single, anterior bending couple rather than with distributed muscles forces. In spite of these deficiencies, MARMT and the BVC generate a startle response that, while slower than that of bony fish (Hale et al. 2002), is similar in gross kinematic pattern of stages 1 and 2 (Fig. 4). In addition, the cruising behavior of MARMT can be compared to other models of undulatory swimmers in which the relation between U and E' is known or predicted. As an undulatory cruiser, MARMT occupies an intermediate position (Fig. 11). Thus, we judge that MARMT swimming with a BVC behaves in a way that is sufficiently fish-like to permit it to be a useful model for testing biological hypotheses.

Summary

As the number of vertebrae, N, increase in a BVC of fixed length, the stiffness of the vertebral column, measured as the storage modulus, E' (MPa), increases, and that mechanical change, in turn, alters swimming behavior. It does so for peak acceleration during a startle and for mean speed during cruising, with our BVC operating as the primary propulsive element in a self-propelled undulatory robot called MARMT. Thus, in a physically-embodied, fully-dynamic robotic model, we show a direct connection between morphology, mechanical properties, and locomotor behavior (Fig. 9).

Acknowledgments

We thank the organizers of the symposium, Brooke Flammang and Marianne Porter, for the invitation to participate. Tom Koob has been our long-term collaborator on BVCs, and much of this work can be traced back to his influences. Randy Ewoldt provided important critiques of our bending tests. Sindre Grotmol provided stimulating discussions about the abutment of vertebrae. Carl Bertsche and Gianna McArthur were instrumental in designing, building, and testing the custom bending rig. Carina Frias was an important member of the team conducting the MARMT experiments. MARMT is a child of the autonomous Tadro robot, and the inventors of the original Tadro and its descendents deserve credit: Hugh Crenshaw, Nicole Doorly, Mathieu Kemp, Adam Lammert, Nick Livingston, Matt McHenry, Charles Pell, Joe Schumacher, and Jim Strother. We thank Kira Irving, Foster Ranney, Hannah Rosenblum, Elise Stickles, Josh Sturm, for help designing, building, and testing BVCs.

Funding

National Science Foundation of the United States of America (DBI-0442269 and IOS-0922605).

References

Brainerd EL, Patek SN. 1998. Vertebral column morphology, c-start curvature, and the evolution of mechanical defenses in tetraodontiform fishes. Copeia 1998:971–84.

Brooks R. 2000. Artificial life: from robot dreams to reality. Nature 406:945–7.

Doorly N, Irving K, McArthur G, Combie K, Engel V, Sakhtah H, Stickles E, Rosenblum H, Gutierrez A, Root R, Liew C-W, Long JH Jr. 2009. Biomimetic evolutionary analysis: robotically-simulated vertebrates in a predator-prey ecology. Proceedings of the 2009 IEEE Symposium on Artificial Life, 147–54.

Fish FE. 2006. Limits of nature and advances of technology: what does biomimetics have to offer to aquatic robots? Appl Bionics Biomech 3:49–60.

Grotmol S, Nordvik K, Hryvi H, Totland G. 2005. A segmental pattern of alkaline phosphatase activity within the notochord coincides with the initial formation of the vertebral bodies. J Anat 206:427–36.

Hale ME, Long JH Jr, McHenry MJ, Westneat MW. 2002. Evolution of behavior and neural control of the fast-start escape response. Evolution 56:993–1007.

Koob TJ, Long JH Jr. 2000. The vertebrate body axis: evolution and mechanical function. Am Zool 40:1–18.

Krishnamurthy P, Khorrami F, de Leeuw J, Porter M, Livingston K, Long JH Jr. 2010. An electric ray inspired biomimetic autonomous underwater vehicle. Proceedings of the American Control Conference, 5224–9.

Lauder GV, Anderson EJ, Tangorra J, Madden PGA. 2007. Fish biorobotics: kinematics and hydrodynamics of self-propulsion. J Exp Biol 210:2767–80.

Lauder GV, Madden PGA. 2006. Learning from fish: kinematics and experimental hydrodynamics for roboticists. Int J Autonomation Comp 4:325–35.

Librizzi NN, Long JH Jr, Root RG. 1999. Modeling a swimming fish with an initial-boundary value problem: unsteady maneuvers of an elastic plate with internal force generation. Math Comput Model 30:77–93.

Long JH Jr. 1992. Stiffness and damping forces in the intervertebral joints of blue marlin (Makaira nigricans). J Exp Biol 162:131–55.

Long JH Jr. 1998. Muscles, elastic energy, and the dynamics of body stiffness in swimming eels. Am Zool 38:771–92.

Long JH Jr. 2007. Biomimetic robotics: building autonomous, physical models to test biological hypotheses. Procs Inst Mech Engineers, Part C, J Mech Eng Sci 221:1193–200.

Long JH Jr. 2011. Biomimetics – robotics based on fish swimming. In: Farrell AP, Cech JJ, Richards JG, Stevens ED, editors. Encyclopedia of fish physiology: from genome to environment. San Diego, CA: Elsevier Academic Press.

Long JH Jr, Adcock B, Root RG. 2002. Force transmission *via* axial tendons in undulating fish: a dynamic analysis. Comp Biochem Physiol, Part A 133:911–29.

Long JH Jr, Hale ME, McHenry MJ, Westneat MW. 1996. Functions of fish skin: flexural stiffness and steady swimming of longnose gar, Lepisosteus osseus. J Exp Biol 199:2139–51.

Long JH Jr, Koob TJ, Irving K, Combie K, Engel V, Livingston N, Lammert A, Schumacher J. 2006. Biomimetic evolutionary analysis: testing the adaptive value of vertebrate tail stiffness in autonomous swimming robots. J Exp Biol 209:4732–46.

Long JH Jr, Koob-Emunds M, Koob TJ. 2004. The mechanical consequences of vertebral centra. Bull MDI Biol Lab 43:99–101.

Long JH Jr, Nipper KS. 1996. The importance of body stiffness in undulatory propulsion. Am Zool 36:678–94.

Long JH Jr, Pabst DA, Shepherd WR, McLellan WA. 1997. Locomotor design of dolphin vertebral columns: bending mechanics & morphology of Delphinus delphis. J Exp Biol 200:65–81.

McHenry MJ, Pell CA, Long JH Jr. 1995. Mechanical control of swimming speed: stiffness and axial wave form in an undulatory fish model. J Exp Biol 198:2293–305.

Mehta RS, Ward AB, Alfaro ME, Wainwright PC. 2010. Elongation of the body in eels. Int Comp Biol 50:1091–105.

Nowroozi BN, Brainerd EL. 2010. Lateral bending kinematics of the vertebral column in *Morone saxatilis*. Int Comp Biol 50:E126.

Porter ME, Beltrán JL, Koob TJ, Summers AP. 2006. Material properties and biochemical composition of mineralized vertebral cartilage in seven elasmobranch species (Chondrichthyes). J Exp Biol 209:2920–8.

Porter ME, Long JH Jr. 2010. Vertebrae in compression: mechanical behavior of arches and centra in the gray smooth-hound shark (*Mustelus californicus*). J Morph 271:366–75.

Porter ME, Roque CM, Long JH Jr. 2009. Turning maneuvers in sharks: predicting body curvature from body and vertebral morphology. J Morph 270:954–65.

Schmitz RJ. 1995. Ultrastructure and function of cellular components of the intercentral joint in the percoid vertebral column. J Morph 226:1–24.

Shu D-G, Conway MS, Han J, Zhang Z-F, Yasui K, Janvier P, Chen L, Zhang X-L, Lui J-N, Li Y, Lui H-Q. 2003. Head and backbone of the Early Cambrian vertebrate *Haikouichthys*. Nature 421:526–9.

Summers AP, Long JH Jr. 2006. Skin and bones, sinew and gristle: the mechanical behavior of fish skeletal tissues. In: Shadwick RE, Lauder GB, editors. Fish Biomechanics. Vol. 23. San Diego, CA: Elsevier Academic Press. p. 141–77.

Symmons S. 1979. Notochordal and elastic components of the axial skeleton of fishes and their functions in locomotion. J Zool 189:157–206.

Tangorra JL, Davidson SN, Hunter IW, Madden PGA, Lauder GV, Dong H, Bozkurttas M, Mittal R. 2007. The

development of a biologically inspired propulsor for unmanned underwater vehicles. IEEE J Ocean Engineer 32:533–50.

Tytell ED, Hsu C-Y, Williams TL, Cohen AH, Fauci LJ. 2010. Interactions between internal forces, body stiffness, and fluid environment in a neuromechanical model of lamprey swimming. Proc Nat Acad Sci 107:19832–7.

Wainwright SA, Biggs WD, Currey JD, Gosline JM. 1976. Mechanical design in organisms. Princeton, NJ: Princeton University Press.

Ward A, Brainerd EL. 2007. Evolution of axial patterning in elongate fishes. Biol J Linn Soc 90:97–116.

Ward A, Mehta RS. 2010. Axial elongation in fishes: using morphological approaches to elucidate developmental mechanisms in studying body shape. Int Comp Biol 50:1106–19.

Webb B. 2001. Can robots make good models of biological behaviour? Behav Brain Sci 24:1033–50.

Webb B. 2006. Validating biorobotic models. J Neural Engineer 3:R25–35.

Webb B, Consi TR. 2001. Biorobotics: methods and applications. Cambridge, MA: MIT Press.